Enabling MIMO Radars in WLAN Sensing: From Spatial Multiplexing to Beamsteering

Hasan Can Yildirim*, Laurent Storrer*, Martin Willame*†, Jérôme Louveaux†, François Horlin*
*Université Libre de Bruxelles - †Université Catholique de Louvain

{*hasan.can.yildirim, laurent.storrer, francois.horlin@ulb.be*}*@ulb.be*
{*martin.willame, jerome.louveaux*}*@uclouvain.be*

***Abstract*—This paper explores augmenting MIMO radar capabilities within WLAN Sensing, using existing algorithms and protocols without altering the standard framework. By integrating MU-MIMO precoding for beam steering, the study enhances spatial awareness and radar sensing capabilities. The approach includes a comprehensive signal model for Wi-Fi signals as MIMO radars, proposes a precoder for improved sensing, and validates these methods through numerical analysis and experimental results. The research highlights the potential of leveraging communication technologies for advanced radar sensing applications, offering a significant step forward in WLAN sensing capabilities.**

***Index Terms*—WLAN Sensing, MIMO radars, radar precoding, beamsteering**

I. Introduction

Wireless communication and radar technologies, once distinct, are now converging into joint communication and sensing (JCAS) [1], where a single analog front-end serves both purposes. This convergence, exemplified by WLAN Sensing (IEEE 802.11bf [2]), enables simultaneous or sequential operations by utilizing and leveraging existing communication protocols for wireless sensing to enable applications such as fall detection, heart rate monitoring, and many more [3]. Therefore, it becomes crucial to understand what currently exists in the WLAN standardization to enhance sensing capabilities without adding new technologies.

The WLAN Sensing utilizes synchronization protocols used for multi-user multi-input multi-output (MU-MIMO) [4] since the 802.11ac amendment. In this protocol, the access point (AP) enables each user station (STA) to estimate its MIMO channel through a known Wi-Fi frame called the null data packet (NDP). In essence, this mechanism triggers sensing sessions for radar-like measurements in different geometries. Moreover, WLAN Sensing offers flexibility by defining various roles and modes to sensing devices [2].

In the meantime, a paradigm shift in radar technology occurred with the advent of MIMO radars, employing multiple antennas for simultaneous transmission and reception of diverse, linearly independent waveforms [5]. These systems enable synthesis of transmit beampatterns, spatial multiplexing and creation of virtual arrays to greatly enhance spatial resolution. Techniques such as adjusting the sample covariance matrix [6] and utilizing singular value decomposition [7] and optimization criteria [8] have been developed for waveform design.

In our prior work, WLAN sensing and MIMO radars have been gradually integrated. Initially, the impact of MU-MIMO precoding on the radar coverage have been investigated, particularly in high Rician K-factor scenarios [10]. Subsequently, we demonstrated that knowledge of the precoder matrix facilitates estimation of target angle-of-departure (AoD) through an optimization problem [11].

In this paper, we investigate MIMO radar capabilities in WLAN Sensing and propose methods to improve its capabilities without altering the existing standard. More specifically, we use MU-MIMO precoding to direct beams towards targets more effectively. Our main contributions are developing a full signal model that describes how Wi-Fi signals can function as MIMO radars, introducing a new precoding method to boost sensing performance, and presenting detailed numerical studies to validate our proposed sensing approach.

The vectors and matrices are defined as $\mathbf{x}$ and $\mathbf{X}$, respectively; x^*, $\mathbf{x}^*$ and $\mathbf{X}^*$ represent conjugate of a scalar, Hermitian transpose of a vector and a matrix, respectively.

II. System Model: WI-FI as a MIMO Radar

In this section, the Wi-Fi system model is provided from a MIMO radar perspective. Detailed derivations can be found in [11]. For the sake of simplicity, we denote the OFDM symbols dedicated to sensing in NDPs as Sensing-Long Training Fields (S-LTFs).

A. Transmit Signal

Let x_q be the BPSK symbol mapped on subcarrier q in the S-LTF, while the transmitter (Tx) and the receiver (Rx) are equipped with N_T and N_R antennas, respectively.

In the Wi-Fi standardization, the Tx streams are first orthogonalized in the frequency-domain for SU/MU-MIMO channel estimation by utilizing the following mapping matrices

$$\mathbf{P}_{2\times 2} = \begin{bmatrix} 1 & 1 \\ 1 & -1 \end{bmatrix}, \mathbf{P}_{4\times 4} = \begin{bmatrix} -1 & 1 & 1 & 1 \\ 1 & 1 & 1 & -1 \\ 1 & 1 & -1 & 1 \\ 1 & -1 & 1 & 1 \end{bmatrix}$$

where $\mathbf{P}\mathbf{P}^T = N_T\mathbf{I}$ and $\mathbf{P} = \mathbf{P}^T$ (for larger array sizes, the reader is referred to [**?**].). Moreover, $\mathbf{P}$ enables spatial multiplexing between the Tx and Rx, i.e., Rx can estimate the channel coefficients for each Tx-Rx antenna pairing.

Second, cyclic shift diversity (CSD) is applied on the subcarriers per antenna stream n through a diagonal matrix that is used to rotate the subcarriers, defined as

$$\mathbf{\Lambda}_q = \begin{bmatrix} e^{j2\pi\frac{q\delta_1}{Q}} & \dots & 0 \\ \vdots & \ddots & \vdots \\ 0 & \dots & e^{j2\pi\frac{q\delta_N}{Q}} \end{bmatrix}, \in \mathbb{C}^{N_T\times N_T}.$$

whose elements are defined as $\mathbf{\Lambda}_q[n,n] = e^{j2\pi\frac{q\delta_n}{Q}}$ and the cyclic shift value of the nth Tx antenna is predefined by the standard. The CSD primarly targets the temporaly characteristics of transmitted signals. However, it also influences the effective radiation pattern observed at the Rx due to the phase differences introduced by the time shifts.

Finally, a custom mapping matrix (CMM) $\mathbf{D}_q, \in \mathbb{C}^{N_T\times N_T}$ is applied to the subcarriers which is either i) an identity matrix for any non-MIMO transmission, or ii) the zero-forcing-precoder (ZFP).

Thus, combining these processes yields the following transmit signal on subcarrier q

$$\mathbf{S}_q = \mathbf{D}_q\mathbf{\Lambda}_q\mathbf{P}x_q, \in \mathbb{C}^{N_T\times N_t}. \tag{1}$$

Here, each column of $\mathbf{S}_q$ represents different time instances $N_t = N_T$, i.e., successive S-LTFs, whereas its rows correspond to the different Tx antennas.

To analyze the MIMO radar capabilities of (1), its covariance matrix can be computed [5], yielding

$$\begin{aligned}\boldsymbol{\mathcal{R}}_q = \mathbf{S}_q\mathbf{S}_q^* &= \mathbf{D}_q\mathbf{\Lambda}_q\mathbf{P}x_qx_q^*\mathbf{P}^*\mathbf{\Lambda}_q^*\mathbf{D}_q^* \\ &= \begin{cases} N_T\mathbf{I}, & \mathbf{D}_q = \mathbf{I} \\ N_T\boldsymbol{\mathcal{R}}_{\mathbf{D}_q}, & \mathbf{D}_q \neq \mathbf{I} \end{cases}\end{aligned} \tag{2}$$

where the last equality is obtained since $x_qx_q^* = 1$, $\mathbf{\Lambda}_q\mathbf{\Lambda}_q^* = \mathbf{I}$, and $\mathbf{P}\mathbf{P}^* = N_T\mathbf{I}$. If CMM is an identity matrix, the covariance matrix also reduces to an identity matrix which attributes the best possible cross-correlation property since self-interference is completely omitted. This makes the S-LTFs quite useful for MIMO radar processing, whether it is for enhanced spatial resolution with virtual arrays, distributed MIMO, or improved target signal-to-noise ratio (SNR) [5]. On the other hand, the CMMs can be used to precode the transmit streams for beam steering in MU-MIMO, which may potentially impact the cross-correlation properties as we will be studying in Section IV.

B. Sensing Channel and Receiver Processing

Let us define the sensing matrix (SM) per target k on subcarrier q at slow-time index l as follows

$$\mathbf{H}_{q,l}^k = \begin{bmatrix} h_{q,l,1,1} & \dots & h_{q,l,N_T,1} \\ \vdots & \ddots & \vdots \\ h_{q,l,1,N_R} & \dots & h_{q,l,N_T,N_R} \end{bmatrix}, \in \mathbb{C}^{N_R\times N_T}.$$

For a deterministic sensing channel with only the line-of-sight (LOS), the entries in $\mathbf{H}_{q,l}^k$ are defined as follows

$$\begin{aligned}\mathbf{H}_{q,l}^k[m,n] &= h_{q,l,m,n}^k \\ &= \alpha_k e^{j2\pi\frac{q\tau_k}{QT}} e^{j2\pi f_k l T_i} e^{j\pi(n\sin(\theta_k)+m\sin(\phi_k))}\end{aligned} \tag{3}$$

where Q, T and T_i are the number of subcarriers, the sampling interval and the duration between successive channel measurements, respectively; α_k, τ_k, f_k, θ_k and ϕ_k correspond to the attenuation, propagation delay, Doppler frequency shift and angle-of-departure and angle-of-arrival of target k, respectively. Evidently, these target parameters depend on the radar geometry, whether it is monostatic, or bistatic [12].

The received sensing signal, also known as the surveillance signal, takes the following form

$$\mathbf{R}_{q,l} = \mathbf{H}_{q,l}\mathbf{S}_q + \mathbf{Z}_{q,l}. \tag{4}$$

where $\mathbf{H}_{q,l} = \sum_{k=1}^K \mathbf{H}_{q,l}$. Then, thanks to the spatial multiplexing used at the Tx, the sensing Rx can apply the transmit process in the reverse order to decouple and estimate the MIMO coefficients, yielding

$$\hat{\mathbf{H}}_{q,l} = \mathbf{H}_{q,l} + \mathbf{Z}_{q,l}\mathbf{P}^T\mathbf{\Lambda}_q^* \tag{5}$$

Finally, by applying the following processes, radar parameters of each target can be obtained [11]: i) IFFT over all subcarriers yielding range profiles; ii) FFT along range cells yielding range/Doppler maps, and iii) FFT/MUSIC [15]/ESPRIT [16] on range/Doppler cells yielding angle profiles.

III. Precoding for Enhanced Sensing

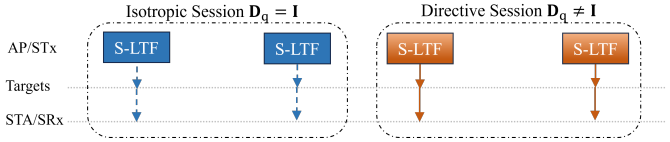

Fig. 1. STx and SRx refers to sensing transmitter and sensing Rx [2], respectively. A bistatic geometry is considered for generality where the AP is the STx, and a user device is the SRx. Depending on the amendment, S-LTF is VHT/HE/EHT-LTF for 802.11ac/11ax/11be, respectively.

To unleash the full potential of WLAN Sensing, we propose leveraging the existing MU-MIMO communication technologies for beam steering. Currently, WLAN Sensing relies on isotropic transmission for target detection. Our suggestion is to utilize MU-MIMO precoding for improved spatial awareness. This approach builds upon a sensing session that already took place using isotropic transmission, as depicted in Fig. 1, where the target parameters are obtained through the radar processing outlined in Section II.

Let $\{\hat{\theta}_k\}_{k=1}^K$ denote the set of coarsely estimated target AoDs, and let us define the direction mapping vector for target k at $\hat{\theta}_k$ as follows

$$\hat{\mathbf{v}}^k = \frac{\mathbf{a}_w(\hat{\theta}_k)}{\left\|\mathbf{a}_w(\hat{\theta}_k)\right\|_2}, \in \mathbb{C}^{N_T\times 1} \tag{6}$$

and the weighted steering vector is defined as

$$\mathbf{a}_w(\hat{\theta}) = \mathbf{a}(\hat{\theta}) \odot \mathbf{w}$$
$$\text{with } \mathbf{a}(\hat{\theta}) = [1 \; e^{j\pi \sin(\hat{\theta})} \; \dots \; e^{j\pi(N_T-1)\sin(\hat{\theta})}]^T / \quad (7)$$

Here, the entries in $\mathbf{w}$ correspond to weights applied for sidelobe suppression, and $\odot$ is the Hadamard product. The AP can now construct the following beam mapping matrix per subcarrier q

$$\hat{\mathbf{B}} = \left[\hat{\mathbf{v}}^1 \; \dots \; \hat{\mathbf{v}}^K\right], \in \mathbb{C}^{N_T \times K} \quad (8)$$

where we omit the index q for clarity. Finally, the AP can compute the ZFP to steer beams towards the targets-of-interest. However, in (1), CSD is applied to the transmit signal, meaning that the beams will be scanning the scene rather than focusing the energy in one direction. In order to avoid this, one can compensate for the CSD matrix and compute the ZFP as follows

$$\hat{\mathbf{D}} = \hat{\mathbf{B}}(\hat{\mathbf{B}}^* \hat{\mathbf{B}})^{-1} \mathbf{\Lambda}^{-1}.$$

where $\mathbf{\Lambda}^{-1}$ is the inverse of the CSD matrix which is trivial to compute since it is a diagonal matrix.

From the standardization perspective, reusing an existing algorithm for a different purpose is advantageous (ZFP is introduced in 802.11ac), since it allows backwards compatibility and eliminates complicated device adaptations. From the MIMO radar perspective, using ZFP for beam steering offers multiple advantages [13], including flexible beamforming control, inter-target-interference suppression, and exploiting spatial multiplexing. On the other hand, its practical implementation entails challenges such as the computational complexity, sensitivity to channel estimation and array calibration errors. Moreover, its applicability is determined by N_T, or degrees of freedom. When $N_T < K$, the pseudo-inverse in Equation (9) becomes rank deficient. Although modern APs typically have multiple Tx antennas (ranging from 2 to 16), the condition $N_T \geq K$ may not always be met, necessitating prioritization of some targets by removing some entries from $\{\hat{\theta}_k\}_{k=1}^K$, e.g., angles that are close in space.

IV. Results

In this section, the proposed method is evaluated for the following standard compliant system parameters: 80 MHz bandwidth, 1024 number of subcarriers, 2.45 GHz carrier frequency, and 23 dBm EIRP. The targets are assumed to have high K-factors, i.e., their LOS dominates all the other multipath components.

The transmit beampattern is evaluated according to the following equation [5]

$$P_{N_T}(\theta) = \mathbf{a}(\theta)^* \boldsymbol{\mathcal{R}}_{\hat{\mathbf{D}}_q} \mathbf{a}(\theta), \quad \theta \in \left[-\frac{\pi}{2}, \frac{\pi}{2}\right]. \quad (9)$$

Here, $\mathbf{a}(\theta)$ is the array steering vector defined in (7) with half-wavelength antenna spacing and $\theta \in \left[-\frac{\pi}{2}, \frac{\pi}{2}\right]$ is the Angle-of-Departure with respect to the linear array.

In Fig. 2, the transmit (Tx) beampatterns are depicted for two array dimensions and varying types of windowing, whilst

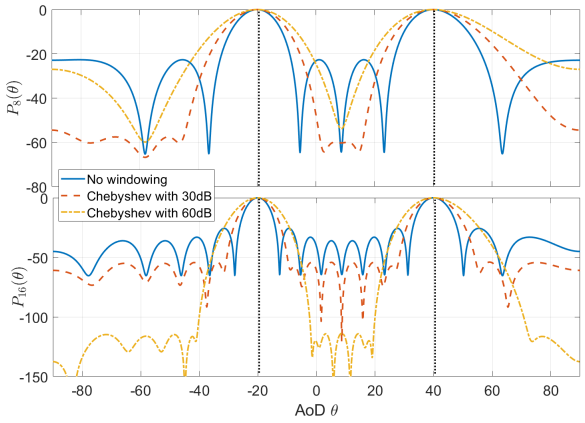

Fig. 2. Transmit beampatterns for different array sizes and types of windowing. Target angles are set to -20 and 40 degrees.

two targets are situated at -20 and 40 degrees. Independent of the array size or the selected windowing method, the beams are accurately oriented towards the intended angular directions. As anticipated, increasing the array size leads narrower beams. Nonetheless, the levels of sidelobes are observed to be considerably elevated (approximately 20 and 35 dB for $N_T = 8$ and $N_T = 16$, respectively), suggesting that other regions within the radar field of view are inadvertently illuminated. To mitigate this issue, Chebyshev windowing is employed within the precoding matrix with two levels of suppression. The efficacy of this windowing technique manifests as it significantly attenuates sidelobe intensities. However, this attenuation incurs an increase in beamwidth, a compromise that is deemed essential particularly within indoor environments.

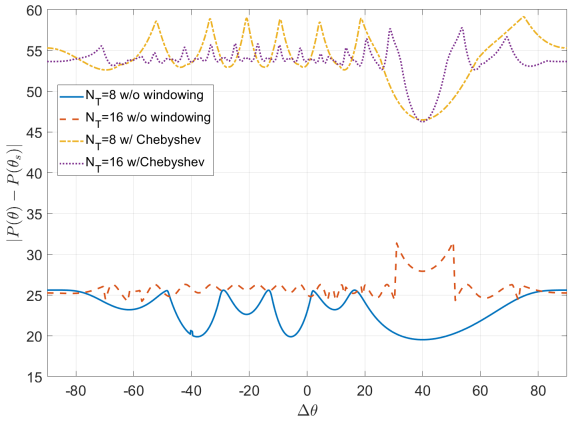

Fig. 3. Sidelobe levels with different array sizes and types of windowing as a function of angular difference between two targets with $\theta_1 = 40$ and $\theta_2 \in [-90, 90]$. The Chebyshev window is adjusted for 30 dB sidelobe suprression.

In Fig. 3, the difference between the mainlobe $P(\theta)$ and the strongest sidelobe $P(\theta_s)$ is shown for different array sizes and types of windowing while the angular separation between two targets is also varied. When no windowing is applied,

the sidelobe levels are around 25 dB while the deviation is approximately 4 dB for $N_T = 8$ and 1 dB for $N_T = 16$. In contrast, when Chebyshev window is used, the difference increases to 55 dB with a deviation of around 3 dB for both array sizes. Moreover, the consistency of the sidelobe suprression is sufficient enough to prove that only the target directions will be illuminated.

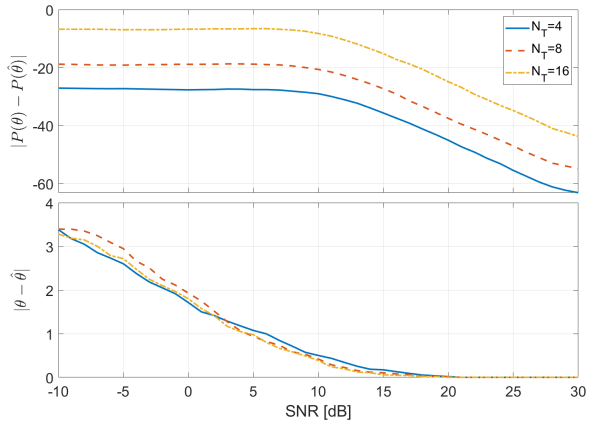

Fig. 4. Impact of angle estimation error on the peak angle and amplitude with Chebyshev window for 30 sidelobe suppression.

The method introduced in Section III starts with a coarse estimation of target angles to shape the transmit beampattern. Fig. 4 illustrates how errors in estimated target angles affect the results, depending on SNR and the antenna array size. The top part of the figure compares the strength of the signal directed at the actual target position, θ, to that aimed at the estimated angle, $\hat{\theta}$. When the SNR is low, the beam does not perfectly line up with the target, leading to a weaker signal at the target. The effect of misalignment is more noticeable with larger arrays since their beams are much narrower and a slight error in where the beam is pointed can result in a big drop in signal strength at the target. However, the difference between the actual and estimated target angles, shown as $\theta - \hat{\theta}$, is mainly influenced by the SNR rather than how big the array is [1]. Notably, at low SNR levels, the accuracy in the beam direction and strength of the beam tends to be lower.

V. Conclusion

This work presents a significant advancement in integrating MIMO radar capabilities within WLAN Sensing, leveraging MU-MIMO precoding for target beam steering without altering existing communication protocols. The proposed method enhances spatial resolution and sensing capabilities by utilizing a novel precoding strategy, validated through comprehensive numerical analyses. The findings underscore the potential of existing WLAN technologies for enhanced radar sensing applications, opening new avenues for research and development in JCAS. This study paves the way for future investigations into optimizing these techniques for various sensing scenarios, highlighting the importance of synergy between communication technologies and radar sensing capabilities.

[1]For larger array sizes, the system inherently attributes better angle estimation accuracy which is not taken into account in simulation to focus only on one effect.

References

[1] Zhang JA, et. al. "An overview of signal processing techniques for joint communication and radar sensing". IEEE Journal of Selected Topics in Signal Processing.

[2] Du R, et. al. "An overview on IEEE 802.11 bf: WLAN sensing". arXiv preprint arXiv:2207.04859. 2022 Jul 11.

[3] Ma, Yongsen, et. al. "WiFi sensing with channel state information: A survey." ACM Computing Surveys (CSUR) 52.3 (2019): 1-36.

[4] Bejarano O, et. al. "IEEE 802.11 ac: from channelization to multi-user MIMO". IEEE Communications Magazine. 2013 Oct 7;51(10):84-90.

[5] Li J, Stoica P. "MIMO radar signal processing". John Wiley & Sons; 2008 Oct 10.

[6] P. Stoica, et. al. "On Probing Signal Design For MIMO Radar," in IEEE Transactions on Signal Processing, vol. 55, no. 8, pp. 4151-4161, Aug. 2007, doi: 10.1109/TSP.2007.894398.

[7] Kirthiga S, et. al. "Transmit beamforming using singular value decomposition". In 2014 International Conference on Electronics and Communication Systems (ICECS) 2014 Feb 13 (pp. 1-4). IEEE.

[8] Huleihel W, et. al. "Optimal adaptive waveform design for cognitive MIMO radar". IEEE Transactions on Signal Processing. 2013 Jun 17;61(20):5075-89.

[9] Mahal JA, et. al. "Spectral coexistence of MIMO radar and MIMO cellular system". IEEE Transactions on Aerospace and Electronic Systems. 2017 Jan 11;53(2):655-68.

[10] Yildirim, Hasan Can, et al. "Impact of MU-MIMO on Passive Wi-Fi Sensing: Threat or Opportunity?." 2022 2nd IEEE International Symposium on Joint Communications & Sensing (JC&S). IEEE, 2022.

[11] Yildirim, Hasan Can, et al. "Passive Wi-Fi-based Radars with 802.11 ax MU-MIMO Signals: AoD Estimation with a Single Antenna." 2023 IEEE 3rd International Symposium on Joint Communications & Sensing (JC&S). IEEE, 2023.

[12] Scheer, Jim, et. al. "Principles of modern radar." (2010).

[13] Fenn, Alan J. Adaptive antennas and phased arrays for radar and communications. Artech House, 2007.

[14] Shadi, Kamal, et. al. "MIMO radar beamforming using orthogonal decomposition of correlation matrix." Circuits, Systems, and Signal Processing 32 (2013): 1791-1809.

[15] Schmidt, Ralph. "Multiple emitter location and signal parameter estimation." IEEE transactions on antennas and propagation 34.3 (1986): 276-280.

[16] R. Roy and T. Kailath, "ESPRIT-estimation of signal parameters via rotational invariance techniques," in IEEE Transactions on Acoustics, Speech, and Signal Processing, doi: 10.1109/29.32276.